Published in final edited form as:
Neuron. 2009 March 26; 61(6): 865–879. doi:10.1016/j.neuron.2009.02.013.

Neurons Detect Increases and Decreases in Oxygen Levels Using Distinct Guanylate Cyclases

Manuel Zimmer[1], **Jesse M. Gray**[1,2], **Navin Pokala**[1], **Andy J. Chang**[1,3], **David S. Karow**[4], **Michael. A. Marletta**[4], **Martin L. Hudson**[5], **David B. Morton**[5], **Nikos Chronis**[1,6], and **Cornelia I. Bargmann**[1]

[1] Howard Hughes Medical Institute, Laboratory of Neural Circuits and Behavior, The Rockefeller University, New York, New York 10065 USA

[4] Departments of Chemistry and Molecular and Cell Biology, The University of California, Berkeley, CA 94720 USA

[5] Department of Integrative Biosciences, Oregon Health & Science University, Portland, OR 97239 USA

Summary

Homeostatic sensory systems detect small deviations in temperature, water balance, pH and energy needs to regulate adaptive behavior and physiology. In *C. elegans,* a homeostatic preference for intermediate oxygen (O_2) levels requires cGMP signaling through soluble guanylate cyclases (sGCs), proteins that bind gases through an associated heme group. Here we use behavioral analysis, functional imaging, and genetics to show that reciprocal changes in O_2 levels are encoded by sensory neurons that express alternative sets of sGCs. URX sensory neurons are activated by increases in O_2 levels, and require the sGCs *gcy-35* and *gcy-36*. BAG sensory neurons are activated by decreases in O_2 levels, and require the sGCs *gcy-31* and *gcy-33*. The sGCs are instructive O_2 sensors, as forced expression of URX sGC genes causes BAG neurons to detect O_2 increases. Both sGC expression and cell-intrinsic dynamics contribute to the differential roles of URX and BAG in O_2 -dependent behaviors.

Introduction

Animals respond to their essential homeostatic needs by adjusting their physiology and by seeking an optimal environment through behavioral strategies. Homeostatic drives that modify behavior include osmosensitive pathways associated with thirst, thermosensory pathways that signal heat and cold, and sensors of internal metabolic states that signal hunger, satiety, nausea, fatigue, and energy imbalances (Craig, 2003; Critchley et al., 2004). Homeostatic sensory systems have needs that are different from those of general sensory systems such as vision or olfaction. First, homeostatic systems operate within a relatively small dynamic range: external signals like light may vary over six orders of magnitude, but internal signals of temperature, pH, or blood sugar must be held in a narrow range, and sensed with similar accuracy. Second,

Correspondence: cori@mail.rockefeller.edu; 212-327-7241.
[2]Current address: Children's Hospital Boston, Harvard Medical School, Boston, MA 02115 USA.
[3]Current Address: Department of Biochemistry and HHMI, Stanford University School of Medicine, Stanford, CA 94305 USA.
[6]Current address: Department of Mechanical Engineering, The University of Michigan, Ann Arbor, MI 48109 USA.

homeostatic systems operate with absolute precision rather than relative precision: in vision or olfaction, changes in stimuli are more important cues than absolute stimulus levels, but a homeostatic system calculates the relationship between the current condition and a defined target condition. The strategies that neuronal homeostatic systems use to calculate these properties are active areas of investigation (Critchley et al., 2004; Pollatos et al., 2007).

Appropriate external and internal O_2 levels are essential for an animal's survival, and central to homeostasis. In air-breathing animals, the lungs and cardiovascular system deliver appropriate O_2 levels to tissues, and the major site of neuronal O_2 sensation is the carotid body, a sensory structure that monitors internal blood levels of O_2, CO_2, and pH through poorly-understood sensory mechanisms (Gonzalez et al., 1994). Animals in aqueous or semi-aqueous environments with variable O_2 levels have additional sensory systems that sense external O_2 levels, as shown for example in *Drosophila*, teleost fish, and *C. elegans* (Gray et al., 2004; Reid and Perry, 2003; Wingrove and O'Farrell, 1999). Neurons that sense internal or external deviations from target O_2 levels can induce general arousal, and can also induce directed behaviors such as hyperventilation, rapid escape behaviors, or aerotaxis behaviors.

The nematode *Caenorhabditis elegans* is found in natural environments such as soil, compost, and rotting fruit where O_2 levels can vary from near-hypoxia to atmospheric levels (Sylvia et al., 1998). *C. elegans* has a strong behavioral preference for ~5–10% O_2. When placed in an O_2 gradient, animals avoid both hypoxia and hyperoxia, suggesting a homeostatic preference for intermediate O_2 levels (Gray et al., 2004). Because of the small size of *C. elegans* and the rapid diffusion of O_2 through tissues, internal O_2 levels are likely to be affected by external conditions; the intermediate preference may optimize the antagonistic requirements to drive oxidative metabolism and avoid oxidative stress (Lee and Atkinson, 1977). Aerotaxis behavior is associated with O_2-induced changes in locomotion speed and turning behavior that may help animals navigate O_2 gradients (Cheung et al., 2005; Gray et al., 2004). The intermediate O_2 preference also promotes aggregation behavior, in part because groups of animals can consume O_2 to generate preferred intermediate O_2 levels (Gray et al., 2004; Rogers et al., 2006).

The strength of the O_2 response is regulated by food, genotype, and an animal's prior experience. The standard wild-type *C. elegans* strain N2 is indifferent to high O_2 when food is present, whereas mutants or natural *C. elegans* isolates with low activity of the neuropeptide receptor gene *npr-1* avoid high O_2 in the presence of food, and therefore aggregate (Gray et al., 2004; Cheung et al., 2005; Rogers et al., 2006). Since all strains avoid high O_2 when food is absent, *npr-1* is not essential for primary O_2 detection, but rather for food regulation. Cultivation conditions also regulate O_2 preference: animals cultivated in hypoxia migrate to lower O_2 levels, and avoid high O_2 regardless of food or *npr-1* genotype (Cheung et al., 2005; Chang and Bargmann, 2008).

Many sensory neurons have been implicated in *C. elegans* O_2 responses, either through direct screens or based on their role in aggregation behavior (Figure 1A and legend). Several sensory neuron classes that express soluble guanylate cyclase homologs (sGCs) stimulate the avoidance of high O_2 levels (neurons called URX, AQR, PQR, SDQ, BDU, ALN, and PLN). URX appears to be the most important member of this group, since its activity is uniquely important for aggregation (Coates and de Bono, 2002), but in aerotaxis URX is redundant with other sGC-expressing neurons (Chang et al., 2006). The sensory neurons ASH, ADL, and ADF also promote avoidance of high O_2 levels, but these cells are not needed after animals are cultivated in hypoxia (Chang et al., 2006; Chang and Bargmann; 2008; Rogers et al., 2006). The complex regulation of O_2 behaviors suggests that the many sensory neurons implicated in aerotaxis likely include some that detect food, stress, or other signals, not just neurons that detect O_2.

sGCs are a class of enzymes that bind gases through heme-nitric oxide and oxygen binding (H-NOX) domains and synthesize the second messenger cGMP from GTP. The seven predicted sGC genes in *C. elegans* belong to two β-like families (Figure S1), which will be called β2-like and β3 sGCs based on prior usage (Morton, 2004b). Three observations suggest that sGCs could have a direct role in O_2 sensation. First, mutations in the sGC genes *gcy-35, gcy-36,* and *gcy-34* disrupt aerotaxis, specifically the avoidance of hyperoxia, without affecting most other behaviors (Chang et al., 2006; Cheung et al., 2005; Gray et al., 2004). Second, misexpression of *gcy-35* and *gcy-36* in AWB neurons that do not normally express sGCs alters O_2 preference in aerotaxis assays (Cheung et al., 2005). Third, unlike the well-characterized α1β1 sGCs that are activated >100-fold by nitric oxide but do not bind O_2, the H-NOX domain of GCY-35 binds O_2 (Denninger and Marletta, 1999; Gray et al., 2004), consistent with a role in O_2 sensation. The H-NOX domains of several fly β3 sGCs also bind O_2, and their cyclase activity is inhibited by O_2 *in vitro* (Huang et al., 2007; Morton, 2004a).

The biochemistry of sGCs is suggestive, but as yet there has been no direct demonstration that the activity of sGC-expressing neurons is regulated by O_2. In addition, it is unclear why *C. elegans* needs seven different sGCs. Here we address the nature of rapid O_2 sensation directly by analyzing sensory properties of two classes of sGC-expressing neurons, the URX neurons, previously implicated in O_2 -evoked behaviors, and the BAG neurons, which we find to be O_2-sensitive regulators of behavior with different properties from URX. We show that URX and BAG are activated by increases and decreases in O_2 levels, respectively, and that each neuron has some sensory properties that are directly defined by sGCs, and other properties that are independent of sGC expression.

Results

Distinct sensory neurons signal O_2 downshifts and upshifts

Many sensory neurons have been implicated in aerotaxis behavior, but in complex gradients it is difficult to determine the exact range of O_2 concentrations that animals experience. To clarify the relationship between sensory neurons and defined O_2 stimuli, we used an assay based on step changes in O_2 levels (Cheung et al., 2005; Gray et al., 2004; Rogers et al., 2006). Freely-moving adult animals from the laboratory wild-type strain N2 were tracked in a small chamber without food, in an air flow that switched between 21% O_2, the atmospheric level, and 10% O_2, the preferred level. Under these circumstances, animals responded to either upshifts or downshifts in O_2 with a transient slowing of locomotion speed (Figure 1B,D) and changes in reversal frequency (Figure 1C,E)(Rogers et al., 2006). The slowing response to O_2 downshift lasted approximately 3 minutes, and was significantly enhanced when animals were food-deprived for an hour or more (Figure 1B,D). The reversal response to O_2 downshift in well-fed animals was biphasic, with a brief suppression followed by increased reversal frequency; in starved animals, only the increase in reversal frequency was observed (Figure 1C,E). Upon O_2 upshift, animals slowed and increased their reversal frequency for less than 30 seconds; these responses were independent of feeding state (Figure 1B–E).

Responses of well-fed animals to O_2 step changes resembled previous studies of wild-type animals in most respects (Cheung et al., 2005; Rogers et al., 2006). Two new observations were the biphasic reversal response upon O_2 downshift and the brief slowing upon O_2 upshift. The basal locomotion speed and reversal rates were comparable to those described in previous studies (Ramot et al., 2008a)(Figure 1 legend). All subsequent experiments were conducted after food deprivation to maximize responses to both O_2 upshift and O_2 downshift, and focused on locomotion speed, the most reliable readout in our assays.

Among the characterized neurons that express sGCs, the URX neurons may be sufficient for some O_2 behaviors, because promoter-cDNA fusions that overlap only in URX rescue

gcy-35 and *gcy-36* mutants (Cheung et al., 2005). However, there is also evidence for redundancy between URX and other O_2-sensing neurons (Chang et al., 2006). To ask which specific O_2 responses require URX, slowing and reversal responses were examined in animals whose URX neurons were killed with a laser microbeam (Bargmann and Avery, 1995). Animals lacking URX neurons did not respond to O_2 upshift, but had a normal or enhanced response to O_2 downshift (Figure 1F,G). Animals in which URX, AQR, and PQR were all killed resembled those in which only URX was killed (data not shown). These results implicate URX in the behavioral responses to O_2 upshift.

The search for additional O_2 –sensing neurons was guided by the observation that animals mutant in the *tax-4* gene, which encodes a subunit of a cGMP-gated sensory channel, were defective in all behavioral responses to O_2 (Figure S2; *tax-4* also had a reduced basal locomotion speed). A survey of *tax-4*-expressing neurons revealed that the two BAG sensory neurons, previously implicated in CO_2 sensation (Bretscher et al., 2008; Hallem and Sternberg, 2008), were required for the response to O_2 downshift. Laser ablation of the BAG neurons caused a specific defect in slowing and reversal responses to O_2 downshift, but did not affect the response to upshift (Figure 1H,I). The combined roles of BAG and URX were sufficient to explain the effect of O_2 on locomotion speed and reversal rates (Figure 1J,K).

URX and BAG neurons sense opposite changes in O_2 levels

Do URX and BAG sense O_2 directly? To move from a behavioral to a functional analysis of O_2 detection, methods were developed to monitor O_2 responses in sensory neurons. *C. elegans* neurons are not thought to generate sodium-based action potentials, but they do have plateau potentials and depolarization events associated with the opening of voltage-activated calcium channels, suggesting that calcium signals can be a reasonable proxy for membrane depolarization (Goodman et al., 1998; Mellem et al., 2008). In several neurons and in muscle, genetically-encoded calcium indicators have generated results qualitatively similar to electrophysiological recordings, albeit less temporally and quantitatively refined (Clark et al., 2007; Kerr et al., 2000; O'Hagan et al., 2005; Raizen and Avery, 1994; Ramot et al., 2008b; Suzuki et al., 2003). To measure intracellular calcium in URX and BAG, the genetically-encoded calcium sensor G-CaMP, whose fluorescence increases upon calcium binding in the physiological range (Nakai et al., 2001; Tallini et al., 2006), was expressed under cell-type selective promoters in URX (G-CaMP1.0) or BAG (G-CaMP2.0). G-CaMP signals in *C. elegans* neurons are similar to those recorded with the ratiometric calcium indicator cameleon (Chronis et al., 2007), but G-CaMP has a larger dynamic range. Animals expressing G-CaMP in URX or BAG had normal behavioral responses to both O_2 upshifts and downshifts (data not shown).

A specialized imaging chamber was designed to deliver O_2 stimuli while recording G-CaMP fluorescence. Adult animals were immobilized in a custom-designed two-layer microfluidic device fabricated of the optically transparent, O_2-permeable polymer polydimethylsiloxane (PDMS) (Figure 2A,B). One layer of the device consisted of a 100 μm thick microfluidic worm immobilization channel (Chronis et al., 2007) (red channel in Figure 2A,B). The second layer of the device contained a gas-flow channel bonded to the top of the worm channel (blue channel), connected via a switch to different gas mixtures. The ~75 μm PDMS partition between the two channels allowed rapid equilibration of O_2 levels in the worm channel. Absolute O_2 levels and switching speed in the worm channel were determined by measuring O_2-induced quenching of the fluorescent dye $Ru(phen)_3Cl_2$ (Klimant and Wolfbeis, 1995) in the device. O_2 downshifts were complete within 10 seconds and upshifts within 5 seconds after switching, verifying the usefulness of the device for stimulus delivery (Figure 2C).

Both URX and BAG neurons responded to O_2 changes with calcium transients. In the URX neurons, a 10–21% O_2 upshift resulted in significant enhancement of G-CaMP fluorescence,

suggesting a calcium increase (Figure 2D). This signal peaked within 6 seconds and decayed over the next 40 seconds of the recording. A 21-10% O_2 downshift resulted in a decrease in URX calcium signals, suggesting inhibition (Figure 2D,E, and legend). In control experiments, switching between gas mixtures of the same oxygen concentration did not evoke calcium transients in URX (Figure S3). These results suggest that URX is activated by an O_2 upshift.

BAG neurons had O_2 responses reciprocal to those of URX (Figure 2G,H and Figure 3). In BAG, minimal changes in fluorescence were observed upon O_2 upshifts (Figure 2G). However, a 21-4% O_2 downshift resulted in large calcium signals, and smaller but significant calcium signals followed a 21-10% O_2 downshift (Figure 2H and Figure 3; controls in Figure S3). These results suggest that BAG is activated by an O_2 downshift.

The salient features of O_2 stimuli for URX and BAG were defined by systematically varying the starting O_2 levels and the target O_2 levels during calcium imaging. In both URX and BAG, the most important variable was the target O_2 level. Strong URX calcium signals were observed when animals were shifted to either 15% or 21% O_2 (Figure 3A,B). Responses were graded in magnitude, so that a large O_2 upshift resulted in larger calcium signals. These results suggest that URX detects and represents a shift to the non-preferred 15–21% O_2 levels, with a secondary effect of the magnitude of the change. Strong BAG calcium signals were observed when animals were shifted to 4% O_2, and weaker responses were observed when animals were shifted to 10% O_2 (Figure 3C,D). The BAG signals were also graded so that a large downshift led to larger responses than a small downshift. These results suggest that BAG primarily detects and represents a shift to a preferred 4–10% O_2 level.

O_2 responses in URX and BAG were sensitive to stimulus history as well as instantaneous O_2 levels. Superimposing traces of $Ru(phen)_3Cl_2$ fluorescence onto analogous traces of calcium signals in URX and BAG showed that strong neural activation correlated with rising and falling O_2 levels, respectively (compare Figure 2C to 2D,H). After oxygen levels reached target values, calcium signals decayed, indicating that URX and BAG, like other sensory neurons, adapt to stimuli over time. Adaptation was not complete after 40 seconds at the target level, since a return to starting levels resulted in a further decrease in signal (Figure 2D,H); these results suggest that an initial strong sensory response is followed by a weaker sustained response. Increasing the holding time at the starting O_2 level increased the magnitude of the subsequent response to a shift, particularly in BAG (Figure S4A–D), demonstrating longer-term adaptation. The time courses of URX and BAG calcium responses were independent of the starting and target O_2 levels (Figure S4E,F). URX neurons had a uniform calcium response, so that each neuron's dynamics over a 60 second trace resembled the averaged trace (Figure 2F); individual BAG neurons had a more complex calcium response that often included secondary peaks (Figure 2I).

sGCs are required for behavioral and neuronal responses to O_2

Previous studies have implicated the *C. elegans* β2-like sGC genes *gcy-34*, *gcy-35*, and *gcy-36* in O_2 dependent behaviors including aerotaxis and the regulation of locomotion speed (Chang et al., 2006; Cheung et al., 2005; Gray et al., 2004). We found that behavioral slowing responses to O_2 upshifts and downshifts required an overlapping but distinct group of four sGC genes: *gcy-31*, *gcy-33*, *gcy-35*, and *gcy-36* (Figure 4). *gcy-35* or *gcy-36* mutants were defective in their behavioral responses to the O_2 upshift, but responded normally to a downshift (Figure 4A,B). *gcy-31* mutants did not respond to the O_2 downshift, but responded normally to an upshift (Figure 4C). *gcy-33* mutants responded poorly to both O_2 downshift and O_2 upshift (Figure 4D).

The behavioral defect in *gcy-35* or *gcy-36* mutants is consistent with their expression in the URX neurons that are required for responses to O_2 upshift (Cheung et al., 2004; Gray et al.,

2004). We found that GFP reporter gene fusions to *gcy-31* were strongly expressed in BAG neurons (Figure S5), which are required for the response to O_2 downshift. A short *gcy-33* promoter fragment is expressed in the BAG sensory neurons (Yu et al., 1997), and we observed that an extended *gcy-33::GFP* reporter gene fusion was expressed in BAG, URX, AQR and PQR neurons (Figure S5). Thus the *gcy- 33, gcy-35,* and *gcy-36* sGC genes required for responses to O_2 upshift overlapped in URX, AQR and PQR neurons, and the *gcy-31* and *gcy-33* sGC genes required for responses to O_2 downshift overlapped in BAG neurons.

The sites of sGC gene function were confirmed by transgenic rescue of *gcy* mutants. The responses of *gcy-35* and *gcy-36* mutants to O_2 upshift were rescued by expressing the appropriate cDNAs under either of two promoters that overlap only in URX (there are no known URX-specific promoters)(Figure 4E,F). The responses of *gcy- 31* and *gcy-33* mutants to O_2 downshift were rescued by expressing *gcy-31* genomic DNA or a *gcy-33* cDNA from BAG-specific promoter sequences (Figure 4G,H). We were unable to rescue the *gcy-33* mutant responses to O_2 upshift with either *gcy-33* genomic clones or cDNA fusions; at this stage the genetic basis of this defect is unclear (see Supplementary material).

An analysis of O_2-evoked calcium responses confirmed and extended conclusions from O_2-evoked behaviors. O_2-evoked calcium signals in URX neurons were abolished in the sGC mutants *gcy-35* and *gcy-36* (Figure 5A,B,F). By contrast, the *gcy-33* mutant strain had a strong O_2-evoked calcium response, despite its defect in URX-mediated behavior (Figure 5C). O_2-evoked calcium signals in BAG neurons were abolished in the sGC mutants *gcy-31* and *gcy-33* (Figure 5D,E,G). These results demonstrate that specific sGCs are required for neuronal sensory calcium transients: GCY-35 and GCY-36 in URX, and GCY-31 and GCY-33 in BAG.

sGCs expressed in URX have been reported to have strong effects on aerotaxis in O_2 gradients (Cheung et al., 2005; Chang et al., 2006), but the functions of sGCs expressed in BAG have not been reported. The behavioral O_2 response controlled by BAG was strongly enhanced by an hour of starvation, so animals were tested for aerotaxis under both well-fed and starved conditions. Well-fed *gcy-31* and *gcy-33* mutants were nearly normal for aerotaxis, but starving animals before the assay uncovered significant defects in the BAG sGC mutants *gcy-31* and *gcy-33* (Figure 6). Like *gcy-35* and *gcy-36*, *gcy-31* and *gcy-33* affected hyperoxia avoidance and not hypoxia avoidance. These results suggest that both the upshift-sensitive neurons and the downshift-sensitive neurons can contribute to aerotaxis in O_2 gradients.

sGCs are instructive sensory molecules

URX and BAG neurons express different sGC genes, and sense different O_2 stimuli. It is interesting to think that the sGCs directly encode quantitative information about O_2 changes, but it is also possible that sGCs have a passive or permissive role in O_2 sensation. To distinguish between active and passive roles for sGCs, we used sGC mutations and transgenes to generate strains in which BAG neurons expressed the sGCs appropriate to URX. First, BAG and URX neurons were functionally inactivated by mutations in endogenous sGCs. Neither BAG nor URX responses were detectable in *gcy-31 gcy-35* double mutants or *gcy-31 gcy-33 gcy-35* triple mutants, as assessed by calcium imaging (Figure 7A,D,F) and behavioral analysis (Figure 8A,C,E). Next, these double and triple mutants were modified by transgenic expression of *gcy-35* and *gcy-36* cDNAs under a BAG-specific promoter.

As predicted if the sGCs are instructive O_2 sensors, the expression of URX sGC genes in BAG transformed its O_2-sensing properties. Calcium signals in the genetically modified BAG neurons increased upon a 4–21% O_2 upshift (Figure 7B,E,F) and decreased upon a 21-4% O_2 downshift (Figure 7C,F). These responses were opposite to normal BAG responses, and resembled normal URX responses.

The apparent exchange of URX sensory coding properties into BAG was confirmed by behavioral analysis of the strains. The *gcy-31 gcy-35* double mutants or *gcy-31 gcy-33 gcy-35* triple mutants expressing *gcy-35* and *gcy-36* in BAG neurons slowed their locomotion upon O_2 upshift, a behavior that would normally be generated by URX neurons and not by BAG neurons (Figure 8B,D,E). Therefore, *gcy-35* and *gcy-36* are sufficient to reprogram BAG neurons to sense an O_2 upshift at a behavioral level.

The correlation between BAG calcium signals and slowing behaviors in wild-type, mutant, and transgenic strains suggests that BAG activation drives slowing behavior. However, calcium is an indirect reporter of neuronal activity, and although calcium transients often accompany depolarization, it seemed useful to obtain a second line of evidence supporting that relationship. To address this issue, the BAG neurons were made light-sensitive by expressing the light-activated depolarizing cation channel channelrhodopsin 2 (ChR2) under a BAG-specific promoter (Nagel et al., 2005). Pulses of blue light led to transient slowed locomotion in BAG*::ChR2* transgenic animals, but not control animals (Figure 8F–H), indicating that depolarization of BAG is sufficient to elicit slowing behavior.

Discussion

A model of O_2 sensation by sGCs

Our results show that two different classes of sensory neurons, URX and BAG, signal the difference between preferred O_2 environments and aversive hyperoxic environments (Figure 8I). URX exhibits calcium transients after an upshift to 15–21% O_2, suggesting that it is depolarized at aversive hyperoxic levels. BAG exhibits calcium transients after a downshift to 4–10% O_2, suggesting that it is depolarized at preferred intermediate O_2 levels. The URX and BAG neurons require distinct sGCs for their opposite responses to O_2; moreover, misexpressing URX sGC genes in BAG transforms the BAG response toward that of URX, both by calcium imaging and by behavior. These results suggest that sGCs are instructive sensors of O_2 downshifts and upshifts.

We suggest that O_2 downshifts increase cGMP production by GCY-31 and GCY-33, allowing opening of the cGMP-gated cation channel encoded by *tax-4* and depolarization of BAG neurons. This model matches biochemical studies of the GCY-31/33-like β3 homologs in *Drosophila*, Gyc-88E and Gyc-89D, whose catalytic activity is inhibited by O_2 *in vitro* (Huang et al., 2007; Morton, 2004a). Conversely, we suggest that O_2 upshifts increase cGMP production by GCY-35 and GCY-36 in URX, perhaps through direct regulation of their enzymatic activity as suggested by the O_2 binding properties of GCY-35 (Gray et al., 2004). The observation that at least two sGC genes are required for O_2-evoked activity in each of the URX and BAG neurons suggests that the sGCs in *C. elegans* may be GCY-35/36 and GCY-31/33 heterodimers, respectively, like NO-sensitive α1β1 sGCs (Denninger and Marletta, 1999). Testing these models will require biochemical reconstitution of *C. elegans* sGC activity, which has not yet been accomplished.

The O_2-binding H-NOX domain is evolutionarily ancient, and is present in O_2- binding proteins in bacteria as well as eukaryotes (Boon and Marletta, 2005). The H- NOX domain is fused to a guanylate cyclase domain in animals and in choanoflagellates, their unicellular ancestors. In animals, sGCs diversified into multiple gene classes (Fitzpatrick et al., 2006)(Figure S1). The *C. elegans* β3 sGCs *gcy-31* and *gcy-33* have homologs in cnidarian, arthropod and fish genomes, and *C. elegans* β2-like sGCs *gcy-35* and *gcy-36* are distantly related to β2 sGCs in vertebrates, whose functions are unknown. It will be interesting to see if other sGCs can detect O_2. The β2-like sGC class expanded from one gene to five genes in nematodes, which have robust O_2 dependent behaviors (Figure S1). Nematodes are notable for their ability to exploit

both high-O_2 and low-O_2 environments; perhaps different sGCs can represent specific O_2 intervals, or sense other gases or internal signals.

BAG and URX neurons have distinct, regulated sensory properties

Both URX and BAG sense O_2, but each neuron has unique behavioral features. URX affects behaviors similarly in well-fed or starved animals, whereas BAG is more important in starved animals. The behavioral response to O_2 stimuli sensed by URX has a time constant of ~16 seconds, compared to a ~113 second time constant for stimuli sensed by BAG. Expression of *gcy-35* and *gcy-36* in BAG results in an intermediate-length behavioral response (τ=46–86 s), suggesting that the timescale of behavior is specified in part by the BAG neurons, and not just by the expression of certain sGCs. The secondary calcium transients observed in BAG are an intriguing feature that may relate to its longer-lasting behavioral effects. Activation of BAG by channelrhodopsin caused a very brief slowing response (τ~11 s), suggesting either that channelrhodopsin inactivates quickly *in vivo*, or that direct depolarization does not fully mimic natural stimuli that activate BAG.

In wild-type animals, URX neurons drive transient slowing behaviors upon an O_2 upshift. URX appears to have a different function in mutants or wild strains with low activity of the *npr-1* neuropeptide receptor: these strains respond to an O_2 downshift with a sustained slowing of locomotion speed that requires URX, *gcy-35*, and *gcy-36*, and is regulated by food (Cheung et al., 2005; Rogers et al., 2006). In all genotypes, the basal locomotion speed of animals lacking URX function is similar to the speed of wild-type animals, suggesting that URX is involved in speed regulation rather than coordinated movement (Coates and de Bono, 2002; this work). Thus URX-dependent speed responses are qualitatively different in wild-type animals (transient slowing to upshift) and *npr-1* animals (sustained slowing to downshift). This difference is specific to speed control: both wild-type animals and *npr-1* mutants increase reversal rates upon O_2 upshift, and in both cases the response requires *gcy-35*, *gcy-36*, and probably URX neurons (Rogers et al., 2006). The regulation of URX information transfer by *npr-1* presents intriguing opportunities for future studies.

In starved wild-type animals, BAG neurons drive transient slowing behavior upon an O_2 downshift. The BAG neurons have also been implicated in behavioral avoidance of carbon dioxide (CO_2) (Bretscher et al., 2008; Hallem and Sternberg, 2008). Although both O_2 and CO_2 sensing properties of BAG require the cGMP-gated channel TAX-4, there are several differences between these sensory properties. O_2 sensing requires *gcy- 31* and *gcy-33*, but CO_2 sensing does not (Hallem and Sternberg, 2008); O_2 sensing is enhanced by starvation, but CO_2 sensing is suppressed by starvation (Bretscher et al., 2008). One *C. elegans* neuron was recently shown to have both olfactory and temperature-sensing properties (Biron et al., 2008; Kuhara et al., 2008); BAG adds a new dimension to sensory flexibility in its apparent ability to switch between different gas- sensing properties based on feeding state.

Homeostatic responses to sensory upshifts and downshifts

There are conceptual analogies between O_2 sensation, studied here, and thermosensation, the best-understood neuronal homeostatic system. In each case, preference is encoded across an array of related sensory molecules, not by a single molecule with an optimum response. Thermosensation in mammals and insects requires thermosensitive cation channels of the TRP superfamily. In mammals, unpleasantly cool temperatures open TRPM8 cation channels in sensory neurons, leading to cold aversion (Bautista et al., 2007; Dhaka et al., 2007), and unpleasantly warm temperatures open TRPV cation channels in sensory neurons and epithelial cells (Caterina et al., 2000; Lee et al., 2005; Moqrich et al., 2005). *Drosophila* also uses multiple temperature-sensitive TRP channels for thermosensation: TRPA1 for slightly elevated temperatures, the TRPA-like Painless channel for higher, noxious heat, and the TRPC family

members TRP and TRPL for cool temperatures (Rosenzweig et al., 2005; Rosenzweig et al., 2008; Tracey et al., 2003).

Similarly, precise O_2 sensation in *C. elegans* requires families of sensory sGC molecules, and multiple sGC-expressing sensory neurons recognize distinct O_2 signals. We have defined the sensory properties of URX and BAG, which correlate with aversive hyperoxic or preferred O_2 levels, but there are several additional sGC-expressing neurons that could also affect the O_2 response (Figure 1A). At the other end of the O_2 range, hypoxia-sensing neurons remain to be identified. Moreover, strong O_2 responses require neurons that may not be directly O_2-sensitive, such as the TRPV-expressing ASH, ADL, and ADF sensory neurons.

An explanation for these sensory processes will require more sophisticated behavioral models, perhaps guided by comparisons between different behaviors. Different *C. elegans* chemosensory neurons have been shown to sense upshifts (URX, ASEL), downshifts (BAG, ASER, AWC), or both changes (ASH) (Chalasani et al., 2007; Chronis et al., 2007; Hilliard et al., 2005; Suzuki et al., 2008). The sensory properties of these neurons are at one level determined by specific sensory molecules like sGCs, which are known only in some cases. However, at a deeper level the sensory properties in a particular neuron or set of functionally-linked neurons may be related to dissimilar behavioral requirements and strategies: rapid escape behaviors for ASH, chemotaxis to the peak of a gradient for ASE and AWC, or aerotaxis to an optimal, intermediate O_2 goal for BAG and URX. Theoretical analysis of circuit motifs suggests that the best strategies for chemotaxis up a gradient are different from the best strategies for finding an optimal concentration (Dunn et al., 2007). Optimum-seeking appears to be the more complex calculation that may need more neurons with different dynamics. Using the models suggested by Dunn et al., we can speculate that the brief slowing and reversals triggered by URX represent an escape-like response that helps animals leave noxious hyperoxia, whereas the prolonged slowing response and multiple reversals triggered by BAG can trap animals in the preferred region where BAG is active. The experimental tractability of *C. elegans* presents an opportunity to match defined neuronal properties to theoretical models, allowing such models to be challenged, tested and refined.

Experimental Procedures

Standard methods were used for genetics and molecular biology. Detailed information on strains, plasmids, and transgenic rescue is included in Supplementary material.

Oxygen flow assays and behavioral analysis

A custom-fabricated plexiglass frame with a flow area of 30 mm × 30 mm × 0.3 mm was sealed on one side with a glass slide. An inlet to the flow chamber was connected to a multi-valve positioner (MVP) (Hamilton RS-232). Pressurized oxygen gases (21% O_2 +/− 2% and 10% O_2 +/− 2%, balanced with nitrogen; GTS-Welco) were passed from the tanks through gas washing cylinder bottles (PYREX) containing distilled water and flow meters (Cole Parmer EW-32121-16) before entering the MVP. Flow rates were set to 50 mL/min. The MVP was controlled by MatLab software (The MathWorks) and configured so that both gas mixtures flowed constantly but only one at a time led into the flow chamber. For each experiment, a 9 cm piece of Whatman filter paper with a 28 mm × 28 mm square arena cut out of the center was soaked in 20 mM $CuCl_2$ and placed onto a 10 cm NGM plate. The aversive $CuCl_2$ solution prevented animals from leaving the central arena. Twenty animals (5–20 animals for experiments shown in Figure 1 and Figure S2) were transferred to the assay arena for each assay. The Plexiglass device was placed onto the assay arena and animals were accustomed to the 21% oxygen gas flow for 5 min. Recordings were made at 3 fps on a digital camera (Pixelink PL-A741, set to binning 2) connected to a Carl Zeiss Stemi 2000-C stereomicroscope equipped with a 0.3x objective and the 28 mm × 28 mm arena was captured in a 494 × 494 pixel area.

Each experiment was carried out 13–28 times (5–20 animals/experiment) for data shown in Figure 1, and 2–6 times for all other experiments. Movies were analyzed by MatLab-based tracking software as described (Chalasani et al., 2007;Ramot 2008a). Animals are detected as areas of defined gray value, and their centroid coordinates are determined for each frame. Centroid positions of adjacent frames are connected to build trajectories, which are used to calculate instantaneous speed and angular velocity. The instantaneous speed was calculated in bins of 5 seconds, only for animals that were moving forward (i.e. not those that reversed or made sharp-angle turns). To exclude behavioral responses to the $CuCl_2$ solution from the analysis, tracks from animals within 2.46 mm (~ 2 worm lengths) of the filter paper were discarded. Speed change was calculated for each animal that was tracked continuously from 10 seconds before to 20 seconds after the O_2 switch; the difference between the mean speed of the first 10 seconds and last 10 seconds of this period was calculated. Reversals were defined as a change from forward to backward locomotion, and detected based on characteristic changes in angular velocity. Time constants were obtained using an exponential fit algorithm (Prism, GraphPad Software, San Diego CA).

For laser-ablated animals in Figure 1, operated or mock-operated animals were subjected to 2–3 consecutive O_2 downshift/upshift pulses; afterwards animals were recovered on food for 2–12 hours before being analyzed again; this cycle was repeated 3–4 times. Responses to all pulses were averaged.

Aerotaxis assays in a 0–21% O_2 gradient were performed as described previously, in the absence of food (Chang et al., 2006).

Light stimulation of ChR2-expressing animals

L4 stage animals were transferred to NGM agar plates onto which a concentrated OP50 bacterial suspension in M9 media and 50 μM all-trans retinal (Sigma) had been spotted and allowed to dry. After 10–36 hours feeding in the dark, young adults were transferred to an NGM plate, and starved for one hour. ChR2 was activated by a royal blue (455 nm) LED (Optotech) delivering ~35 $\mu W/mm^2$ of power to the agar surface. The LED was controlled by MatLab software. Glare was reduced by a Roscolux #312 filter placed in front of the microscope objective. Behavioral analysis was performed as above. The bin size for calculating speed was 1 second.

Calcium imaging

Imaging devices were constructed by standard soft lithography technologies (Xia and Whitesides, 1998). To create a master mold for the worm channel (Chronis et al., 2007), a 30 μm thick layer of SU-8 2025 was spin cast (3000 rpm, 30 seconds) onto a bare silicon wafer prior to patterning by photolithography. A 100 μm thick layer of pre-polymer mixture (PDMS:Silgard 184; 10:1; Dow Corning) was spin cast onto the mold at 1000 rpm for 30 seconds (spinner model WS-400A-6NPP/LITE/IND; Laurell Technologies Corporation). The master mold for the flow chamber was fabricated from SU-8 50 (MicroChem), which was spin cast at 1500 rpm for 30 seconds onto a bare silicon wafer to obtain a 100 μm thick layer prior to patterning by photolithography. A ~0.75 cm thick layer of the pre-polymer mixture was cast onto this mold. Both casts were cured for 2 hours at 65 °C. The replica of the flow chamber was peeled off and treated together with the replica of the worm channel, which was still attached to the mold, with air plasma (30 W for 30 s). The two PDMS layers were aligned and chemically bonded to each other, peeled off from the mold, inlets and outlets were created with a 0.75 mm “Uni-Core” puncher (Harris), and then the PDMS layers and a coverglass for microscopy (Fisherbrand) were treated with air plasma and chemically bonded to each other.

The gas inlet of the imaging device was attached via a T-connector to two three-way valves (The Lee Company 778360) controlling the intake of two tanks containing pressurized gas premixtures of oxygen and nitrogen (GTS-Welco). The two valves were automatically controlled by the ValveBank 8II (AutoMate Scientific, Inc.). Both gas mixtures were constantly flowing but only one mixture was led into the flow chamber at a time. The gas flow rate was adjusted to yield a pressure of 1.35 +/− 0.05 psi at the outlet of the flow chamber. The worm channel was connected to a reservoir containing S-Basal buffer. All components described above were connected with butyl rubber tubing (0.25 in inner diameter (ID), 0.5 in outer diameter (OD); Fisher Scientific), TYGON tubing (0.02 in ID, 0.06 in OD; Norton) or polyethylene tubing (0.066 in ID x 0.095 in OD; Intramedic) using 23-gauge Luer-stub adapters (Intramedic) and low-pressure fittings (BioRad) of appropriate sizes.

Oxygen levels in the worm channel were measured by filling the channel with a 0.5 mM solution of the oxygen sensitive fluorescent dye $Ru(phen)_3Cl_2$ (Fluka) in ethanol (Klimant and Wolfbeis, 1995). To calibrate the device, it was disconnected from the gas sources and placed in a Petri dish that was flushed with gas mixtures of 0%, 4%, 10%, 15% and 21% O_2. After a few minutes of equilibration, fluorescence intensities were measured by epifluorescence microscopy on a Zeiss Axioskop 2 FS plus microscope with a 10x objective, a Coolsnap HQ CCD camera (Photometrics), a “Piston-GFP” band pass filter set (Chroma), a 0.6 ND neutral density filter (Chroma) and MetaMorph software (Molecular Devices). After these calibration measurements the device was equilibrated to room air and reconnected to the gas sources. Fluorescence intensities were measured on the same microscope by stream acquisition while switching between the different gas mixtures that were passed through the flow chamber. The fluorescence intensities 5–10 seconds after switching were nearly identical to the ones obtained during the calibration measurements. Thus, no measurable losses occurred.

For G-CaMP imaging, animals were loaded into the worm channel in S-Basal medium and calcium levels in neurons were measured and quantified as described previously (Chalasani et al., 2007; Chronis et al., 2007). Animals were transferred to a drop of S-basal buffer on a food-free NGM plate and sucked into Tygon tubing, which was subsequently connected to the worm inlet. By application of a brief vacuum at the worm outlet, animals were loaded into the worm channel. During recordings, animals were submerged in S-Basal buffer at all times. G-CaMP fluorescence was imaged as above but with a 40x “Fluar” oil immersion objective, a 1.3 ND neutral density filter and the camera binning set to 2. Time stacks were acquired by stream acquisition using 100ms exposure time. We recorded from each individual animal once or twice. A script written in MetaMorph programming language was used to analyze stacks. G-CaMP expressing neurons were marked by a region of interest (ROI) determined by thresholding and their position in each frame was tracked using the “Track Objects” function in MetaMorph. An adjacent ROI in each frame was used to subtract background from the total integrated fluorescence intensity of the thresholded area. $\Delta F/F_0$ was calculated as the percent change in fluorescence relative to the mean basal fluorescence (F_0) from 1–4 seconds of each recording.

Before BAG imaging, animals were starved for 1–3 hours on a food-free NGM plate containing a $CuCl_2$ soaked filter paper as described above for behavioral assays, and then loaded into the device.

Supplementary Material

Refer to Web version on PubMed Central for supplementary material.

Acknowledgments

We thank Stanislas Leibler for the use of his clean room facility, the *C. elegans* Knockout Consortium for strains, Leslie B. Vosshall, Sreekanth H. Chalasani, Jennifer Garrison, Elizabeth Glater, Andrés Bendesky, Bluma Lesch, Andrew Gordus, Patrick McGrath, Tanja A. Schwickert, Marc-Werner Dobenecker and all Bargmann laboratory members for critical help, insight and advice. M.Z. was supported by the International Human Frontier Science Program Organization and a Robert Leet and Clara Guthrie Patterson Trust Postdoctoral Fellowship in Brain Circuitry. This work was supported by the Howard Hughes Medical Institute (C.I.B.) and by NIH grant NS29740 (D.B.M.). C.I.B. is an Investigator of the Howard Hughes Medical Institute.

References

Bargmann CI, Avery L. Laser killing of cells in *Caenorhabditis elegans*. Methods Cell Biol 1995;48:225–250. [PubMed: 8531727]

Bautista DM, Siemens J, Glazer JM, Tsuruda PR, Basbaum AI, Stucky CL, Jordt SE, Julius D. The menthol receptor TRPM8 is the principal detector of environmental cold. Nature 2007;448:204–208. [PubMed: 17538622]

Biron D, Wasserman S, Thomas JH, Samuel AD, Sengupta P. An olfactory neuron responds stochastically to temperature and modulates *Caenorhabditis elegans* thermotactic behavior. Proc Natl Acad Sci U S A 2008;105:11002–11007. [PubMed: 18667708]

Boon EM, Marletta MA. Ligand discrimination in soluble guanylate cyclase and the H-NOX family of heme sensor proteins. Curr Opin Chem Biol 2005;9:441–446. [PubMed: 16125437]

Bretscher AJ, Busch KE, de Bono M. A carbon dioxide avoidance behavior is integrated with responses to ambient oxygen and food in *Caenorhabditis elegans*. Proc Natl Acad Sci U S A 2008;105:8044–8049. [PubMed: 18524954]

Caterina MJ, Leffler A, Malmberg AB, Martin WJ, Trafton J, Petersen-Zeitz KR, Koltzenburg M, Basbaum AI, Julius D. Impaired nociception and pain sensation in mice lacking the capsaicin receptor. Science 2000;288:306–313. [PubMed: 10764638]

Chalasani SH, Chronis N, Tsunozaki M, Gray JM, Ramot D, Goodman MB, Bargmann CI. Dissecting a circuit for olfactory behaviour in *Caenorhabditis elegans*. Nature 2007;450:63–70. [PubMed: 17972877]

Chang AJ, Bargmann CI. Hypoxia and the HIF-1 transcriptional pathway reorganize a neuronal circuit for oxygen-dependent behavior in *Caenorhabditis elegans*. Proc Natl Acad Sci U S A 2008;105:7321–7326. [PubMed: 18477695]

Chang AJ, Chronis N, Karow DS, Marletta MA, Bargmann CI. A Distributed Chemosensory Circuit for Oxygen Preference in *C. elegans*. PLoS Biol 2006;4:1588–1602.

Cheung BH, Arellano-Carbajal F, Rybicki I, de Bono M. Soluble guanylate cyclases act in neurons exposed to the body fluid to promote *C. elegans* aggregation behavior. Curr Biol 2004;14:1105–1111. [PubMed: 15203005]

Cheung BH, Cohen M, Rogers C, Albayram O, de Bono M. Experience-Dependent Modulation of *C. elegans* Behavior by Ambient Oxygen. Curr Biol 2005;15:905–917. [PubMed: 15916947]

Chronis N, Zimmer M, Bargmann CI. Microfluidics for in vivo imaging of neuronal and behavioral activity in *Caenorhabditis elegans*. Nat Methods 2007;4:727–731. [PubMed: 17704783]

Clark DA, Gabel CV, Gabel H, Samuel AD. Temporal activity patterns in thermosensory neurons of freely moving *Caenorhabditis elegans* encode spatial thermal gradients. J Neurosci 2007;27:6083–6090. [PubMed: 17553981]

Coates JC, de Bono M. Antagonistic pathways in neurons exposed to body fluid regulate social feeding in *Caenorhabditis elegans*. Nature 2002;419:925–929. [PubMed: 12410311]

Craig AD. Interoception: the sense of the physiological condition of the body. Curr Opin Neurobiol 2003;13:500–505. [PubMed: 12965300]

Critchley HD, Wiens S, Rotshtein P, Ohman A, Dolan RJ. Neural systems supporting interoceptive awareness. Nat Neurosci 2004;7:189–195. [PubMed: 14730305]

Denninger JW, Marletta MA. Guanylate cyclase and the .NO/cGMP signaling pathway. Biochim Biophys Acta 1999;1411:334–350. [PubMed: 10320667]

Dhaka A, Murray AN, Mathur J, Earley TJ, Petrus MJ, Patapoutian A. TRPM8 is required for cold sensation in mice. Neuron 2007;54:371–378. [PubMed: 17481391]

Dunn NA, Conery JS, Lockery SR. Circuit motifs for spatial orientation behaviors identified by neural network optimization. J Neurophysiol 2007;98:888–897. [PubMed: 17522174]

Fitzpatrick DA, O'Halloran DM, Burnell AM. Multiple lineage specific expansions within the guanylyl cyclase gene family. BMC Evol Biol 2006;6:26. [PubMed: 16549024]

Gonzalez C, Almaraz L, Obeso A, Rigual R. Carotid body chemoreceptors: from natural stimuli to sensory discharges. Physiol Rev 1994;74:829–898. [PubMed: 7938227]

Goodman MB, Hall DH, Avery L, Lockery SR. Active currents regulate sensitivity and dynamic range in *C. elegans* neurons. Neuron 1998;20:763–772. [PubMed: 9581767]

Gray JM, Karow DS, Lu H, Chang AJ, Chang JS, Ellis RE, Marletta MA, Bargmann CI. Oxygen sensation and social feeding mediated by a *C. elegans* guanylate cyclase homologue. Nature 2004;430:317–322. [PubMed: 15220933]

Hallem EA, Sternberg PW. Acute carbon dioxide avoidance in *Caenorhabditis elegans*. Proc Natl Acad Sci U S A 2008;105:8038–8043. [PubMed: 18524955]

Hilliard MA, Apicella AJ, Kerr R, Suzuki H, Bazzicalupo P, Schafer WR. In vivo imaging of *C. elegans* ASH neurons: cellular response and adaptation to chemical repellents. Embo J 2005;24:1489.

Huang SH, Rio DC, Marletta MA. Ligand binding and inhibition of an oxygen-sensitive soluble guanylate cyclase, Gyc-88E, from *Drosophila*. Biochemistry 2007;46:15115–15122. [PubMed: 18044974]

Kerr R, Lev-Ram V, Baird G, Vincent P, Tsien RY, Schafer WR. Optical imaging of calcium transients in neurons and pharyngeal muscle of *C. elegans*. Neuron 2000;26:583–594. [PubMed: 10896155]

Klimant I, Wolfbeis OS. Oxygen-sensitive luminescent materials based on silicone-soluble ruthenium diimine complexes. Anal Chem 1995;67:3160–3166.

Kuhara A, Okumura M, Kimata T, Tanizawa Y, Takano R, Kimura KD, Inada H, Matsumoto K, Mori I. Temperature sensing by an olfactory neuron in a circuit controlling behavior of *C. elegans*. Science 2008;320:803–807. [PubMed: 18403676]

Lee, DL.; Atkinson, HJ. Physiology of Nematodes. Vol. 2. New York: Columbia University Press; 1977.

Lee H, Iida T, Mizuno A, Suzuki M, Caterina MJ. Altered thermal selection behavior in mice lacking transient receptor potential vanilloid 4. J Neurosci 2005;25:1304–1310. [PubMed: 15689568]

Mellem JE, Brockie PJ, Madsen DM, Maricq AV. Action potentials contribute to neuronal signaling in *C. elegans*. Nat Neurosci 2008;11:865–867. [PubMed: 18587393]

Moqrich A, Hwang SW, Earley TJ, Petrus MJ, Murray AN, Spencer KS, Andahazy M, Story GM, Patapoutian A. Impaired thermosensation in mice lacking TRPV3, a heat and camphor sensor in the skin. Science 2005;307:1468–1472. [PubMed: 15746429]

Morton DB. Atypical soluble guanylyl cyclases in *Drosophila* can function as molecular oxygen sensors. J Biol Chem 2004a;279:50651–50653. [PubMed: 15485853]

Morton DB. Invertebrates yield a plethora of atypical guanylyl cyclases. Mol Neurobiol 2004b;29:97–116. [PubMed: 15126679]

Nagel G, Brauner M, Liewald JF, Adeishvili N, Bamberg E, Gottschalk A. Light activation of channelrhodopsin-2 in excitable cells of *Caenorhabditis elegans* triggers rapid behavioral responses. Curr Biol 2005;15:2279–2284. [PubMed: 16360690]

Nakai J, Ohkura M, Imoto K. A high signal-to-noise Ca(2+) probe composed of a single green fluorescent protein. Nat Biotechnol 2001;19:137–141. [PubMed: 11175727]

O'Hagan R, Chalfie M, Goodman MB. The MEC-4 DEG/ENaC channel of *Caenorhabditis elegans* touch receptor neurons transduces mechanical signals. Nat Neurosci 2005;8:43–50. [PubMed: 15580270]

Pollatos O, Schandry R, Auer DP, Kaufmann C. Brain structures mediating cardiovascular arousal and interoceptive awareness. Brain Res 2007;1141:178–187. [PubMed: 17296169]

Raizen DM, Avery L. Electrical activity and behavior in the pharynx of *Caenorhabditis elegans*. Neuron 1994;12:483–495. [PubMed: 8155316]

Ramot D, Johnson BE, Berry TL Jr, Carnell L, Goodman MB. The Parallel Worm Tracker: a platform for measuring average speed and drug-induced paralysis in nematodes. PLoS ONE 2008a;3:e2208. [PubMed: 18493300]

Ramot D, MacInnes BL, Goodman MB. Bidirectional temperature-sensing by a single thermosensory neuron in *C. elegans*. Nat Neurosci 2008b;11:908–915. [PubMed: 18660808]

Reid SG, Perry SF. Peripheral O2 chemoreceptors mediate humoral catecholamine secretion from fish chromaffin cells. Am J Physiol Regul Integr Comp Physiol 2003;284:R990–999. [PubMed: 12511426]

Rogers C, Persson A, Cheung B, de Bono M. Behavioral motifs and neural pathways coordinating O2 responses and aggregation in *C. elegans*. Curr Biol 2006;16:649–659. [PubMed: 16581509]

Rosenzweig M, Brennan KM, Tayler TD, Phelps PO, Patapoutian A, Garrity PA. The *Drosophila* ortholog of vertebrate TRPA1 regulates thermotaxis. Genes Dev 2005;19:419–424. [PubMed: 15681611]

Rosenzweig M, Kang K, Garrity PA. Distinct TRP channels are required for warm and cool avoidance in *Drosophila melanogaster*. Proc Natl Acad Sci U S A 2008;105:14668–14673. [PubMed: 18787131]

Suzuki H, Kerr R, Bianchi L, Frokjaer-Jensen C, Slone D, Xue J, Gerstbrein B, Driscoll M, Schafer WR. In vivo imaging of *C. elegans* mechanosensory neurons demonstrates a specific role for the MEC-4 channel in the process of gentle touch sensation. Neuron 2003;39:1005–1017. [PubMed: 12971899]

Suzuki H, Thiele TR, Faumont S, Ezcurra M, Lockery SR, Schafer WR. Functional asymmetry in *Caenorhabditis elegans* taste neurons and its computational role in chemotaxis. Nature 2008;454:114–117. [PubMed: 18596810]

Sylvia, DM.; Fuhrmann, JJ.; Hartel, PG.; Zuberer, DA. Principles and applications of soil microbiology. Upper Saddle River, New Jersey: Prentice Hall; 1998. p. 550

Tallini YN, Ohkura M, Choi BR, Ji G, Imoto K, Doran R, Lee J, Plan P, Wilson J, Xin HB, et al. Imaging cellular signals in the heart in vivo: Cardiac expression of the high-signal Ca2+ indicator GCaMP2. Proc Natl Acad Sci U S A 2006;103:4753–4758. [PubMed: 16537386]

Tracey WD Jr, Wilson RI, Laurent G, Benzer S. painless, a Drosophila gene essential for nociception. Cell 2003;113:261–273. [PubMed: 12705873]

Wingrove JA, O'Farrell PH. Nitric oxide contributes to behavioral, cellular, and developmental responses to low oxygen in *Drosophila*. Cell 1999;98:105–114. [PubMed: 10412985]

Xia Y, Whitesides G. Soft Lithography. Annual Review of Materials Science 1998;28:153–184.

Yu S, Avery L, Baude E, Garbers DL. Guanylyl cyclase expression in specific sensory neurons: a new family of chemosensory receptors. Proc Natl Acad Sci U S A 1997;94:3384–3387. [PubMed: 9096403]

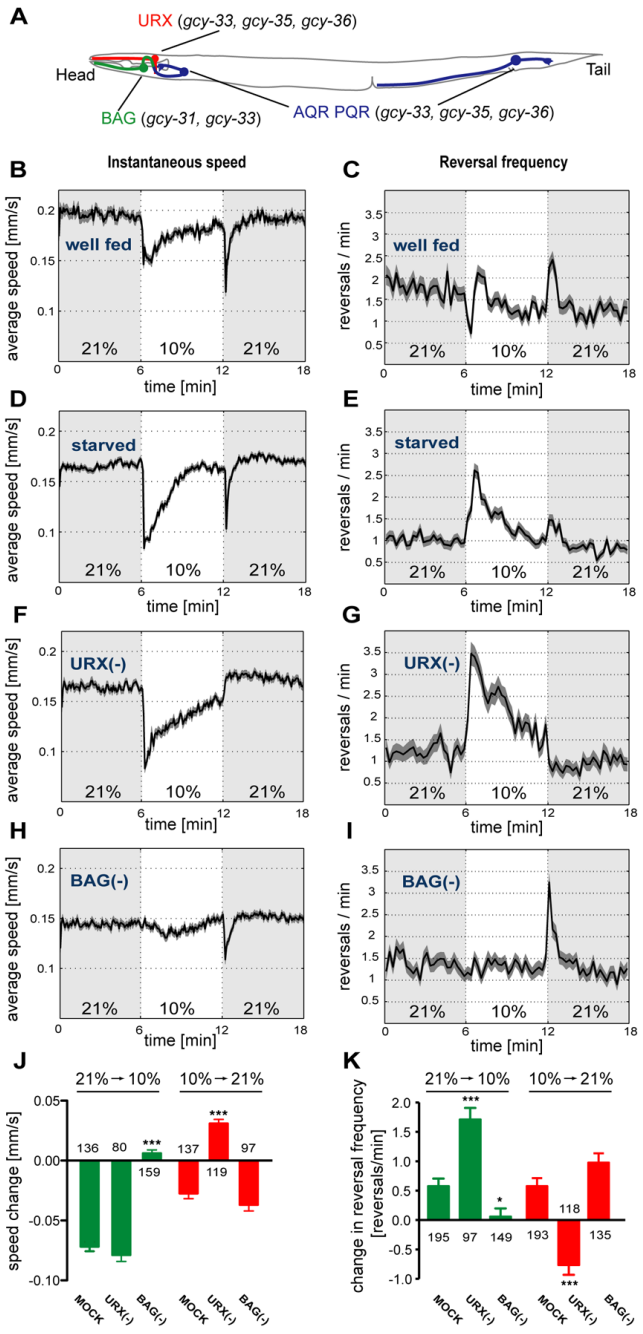

Figure 1. The URX and BAG neurons are required for responses to O_2 upshifts and downshifts

(A) A subset of sGC-expressing sensory neurons of *C. elegans.* Additional sGC-expressing neurons (some of ALN, BDU, SDQ, PLN) and non-sGC expressing sensory neurons (ASH, ADL, ADF) can also affect O_2 responses (Chang et al., 2006; Rogers et al., 2006). **(B–I)** Locomotion speed and reversal rates of *C. elegans* off food. Traces show averages and dark shading indicates standard error of the mean (SEM). Oxygen concentrations were switched between 21% and 10%; light shading marks intervals at 21%. **(B,D,F,H)** Locomotion speed, calculated in 5 second bins. **(C,E,G,I)** Reversals per animal per minute, calculated in 15 second bins. **(B–E)** Wild type animals, well-fed **(B,C)** or 1 hour starved **(D,E).** For well-fed animals, average basal speed was 0.19±0.03 (SD) mm/s, range 0.14–0.28 mm/s; average reversal rate

was 1.5±0.29 (SD) reversals/min, range 0.9–2.1 reversals/min (n=13 assays). For starved animals, average basal speed was 0.17±0.02 mm/s, range 0.13–0.20 mm/s; average reversal rate was 1.1±0.21 reversals/min, range 0.7–1.5 reversals/min (n=21 assays). **(F–I)** animals in which either URX **(F,G)** or BAG **(H,I)** neurons were killed by laser surgery. **(J,K)** Average speed and reversal changes to O_2 upshift and downshift; **(J)** Difference of the mean speeds in 10 seconds before and after the switch; **(K)** Difference in the number of reversals in one minute before and after the switch. Error bars indicate SEM. Asterisks indicate significance by one-way ANOVA with Dunnett's post test using mock-ablated animals as a control group (* P=0.01–0.05, *** P<0.001). The numbers of animal tracks analyzed are indicated.

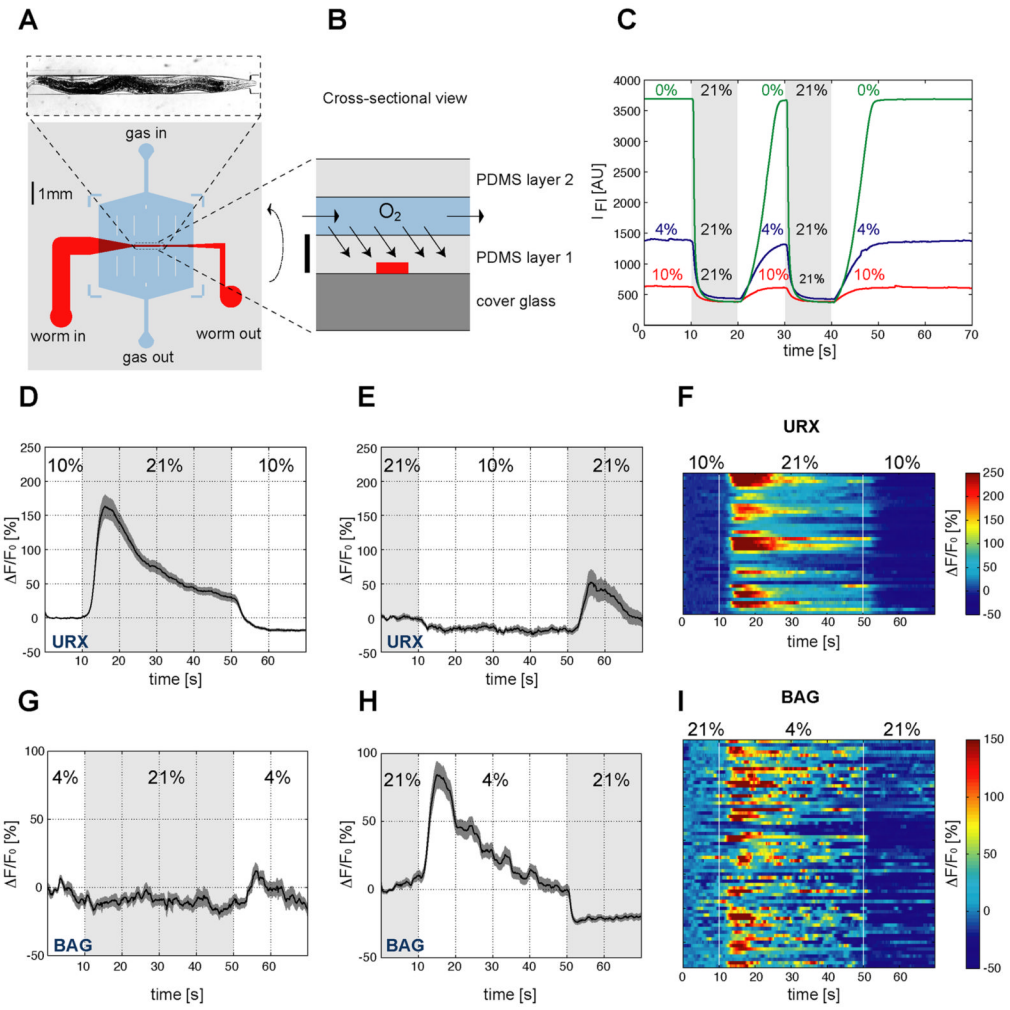

Figure 2. BAG and URX neurons sense O_2

(A,B) Device used to immobilize *C. elegans* for calcium imaging. **(A)** Layout of the microfluidic worm channel (red) and the overlying O_2 flow chamber (blue). The surrounding grey shaded box represents PDMS cast. Image at top shows an animal in the channel. **(B)** Schematic cross section of the device. Scale bar represents 100 μm. **(C)** Fluorescence imaging of the O_2-sensitive dye $Ru(phen)_3Cl_2$ dissolved in the worm channel. Each trace is a fluorescence intensity profile recorded while switching between the indicated O_2 concentrations. **(D–I)** Measurements of neural activity by calcium imaging of URX and BAG. **(D,E,G,H)** Black traces show the average percent change of G-CaMP fluorescence ($\Delta F/F_0$) and dark shading shows standard error of the mean (SEM). Concentrations were 21% and 10% O_2 (**D,E**) or 21% and 4% O_2 (**G,H**). Light grey shading indicates the intervals at 21% O_2. **(D)** Average URX response to O_2 upshift. **(E)** Average URX response to O_2 downshift (a significant decrease is observed following a 21-10% downshift, as compared to a 21-21% control shift (Figure S3) (P=0.0195 by t-test)). **(F)** Individual URX responses to O_2 upshift, n=42. Each row represents one neuron. **(G)** Average BAG response to O_2 upshift. **(H)** Average BAG response to O_2 downshift. **(I)** Individual BAG responses to O_2 downshift, n=67. Each row represents one neuron. Control traces for URX and BAG calcium imaging are shown in Figure S3.

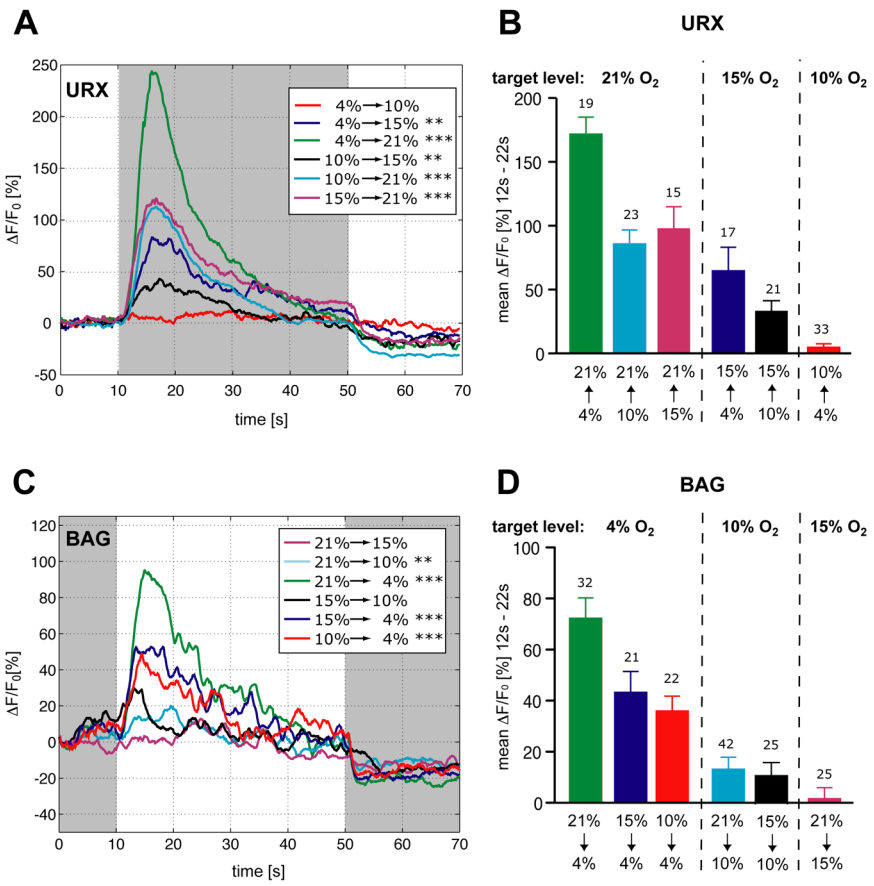

Figure 3. URX and BAG neurons detect concentration shifts within preferred O_2 ranges

Measurements of neural activity by calcium imaging. Traces show the average percent change of G-CaMP fluorescence ($\Delta F/F_0$). **(A)** URX responses. Asterisks indicate significant fluorescence changes comparing mean $\Delta F/F_0$ from 0–10 seconds vs 12–22 seconds (** P=0.001–0.01, *** P<0.001, paired t-test). **(B)** URX average $\Delta F/F_0$ responses (12–22 s), same color code as in (A), arranged to show effects of target O_2 level and O_2 shift magnitude. Error bars indicate SEM. The numbers of recordings analyzed are indicated. **(C)** BAG responses. Asterisks indicate significant fluorescence changes comparing mean $\Delta F/F_0$ from 0–10 seconds vs 12–22 seconds (** P=0.001–0.01, *** P<0.001, paired t-test). **(D)** BAG average $\Delta F/F_0$ responses (12–22 s), same color code as in (C), arranged to show effects of target O_2 level and O_2 shift magnitude. Error bars indicate standard error of the mean (SEM). The numbers of recordings analyzed are indicated. Statistics are in Table S1.

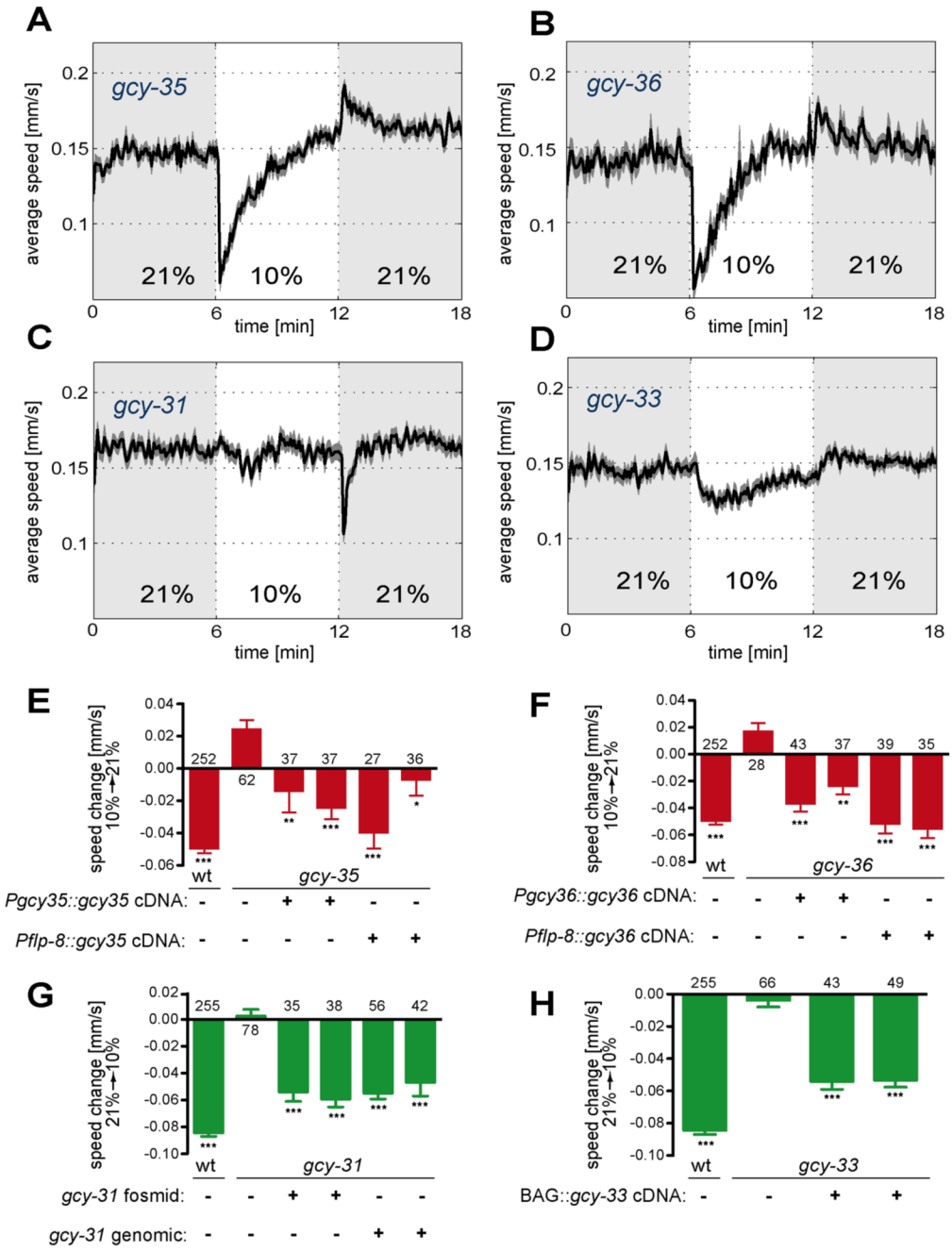

Figure 4. URX and BAG use distinct sGCs to mediate slowing responses to O_2 upshift and downshift

(A–D) Locomotion speed of indicated mutant strains. Traces show average speed and dark shading indicates standard error of the mean (SEM). Oxygen concentrations were switched between 21% and 10%; light grey shading marks intervals at 21%. **(A)** *gcy-35(ok769)* mutants. **(B)** *gcy-36(db66)* mutants. **(C)** *gcy-31(ok296)* mutants. **(D)** *gcy-33(ok232)* mutants. **(E–H)** Average speed changes (differences of the means of 10 second intervals before and after the switch) of animals with indicated genotypes. Error bars indicate SEM. Asterisks indicate significance by one-way ANOVA with Dunnett's post test, using the mutant in each panel as control group (* P=0.01–0.05, ** P=0.001–0.01, *** P<0.001). The numbers of animal tracks analyzed are indicated. Wild type data are from Figure 1D. **(E)** Transgenic rescue of *gcy-35*

(ok769) by a cDNA under its own promoter (expressed in URX, AQR, PQR, BDU, SDQ, AVM, PVM, ALN, and PLN) or the *flp-8* promoter (expressed in URX, AUA, and PVM). **(F)** Transgenic rescue of *gcy-36(db66)* by a cDNA under its own promoter (expressed in URX, AQR and PQR) or the *flp-8* promoter. **(G)** Transgenic rescue of *gcy-31(ok296)* with genomic clones. **(H)** Transgenic rescue of *gcy-33(ok232)* by a cDNA under a BAG-specific *gcy-31* promoter.

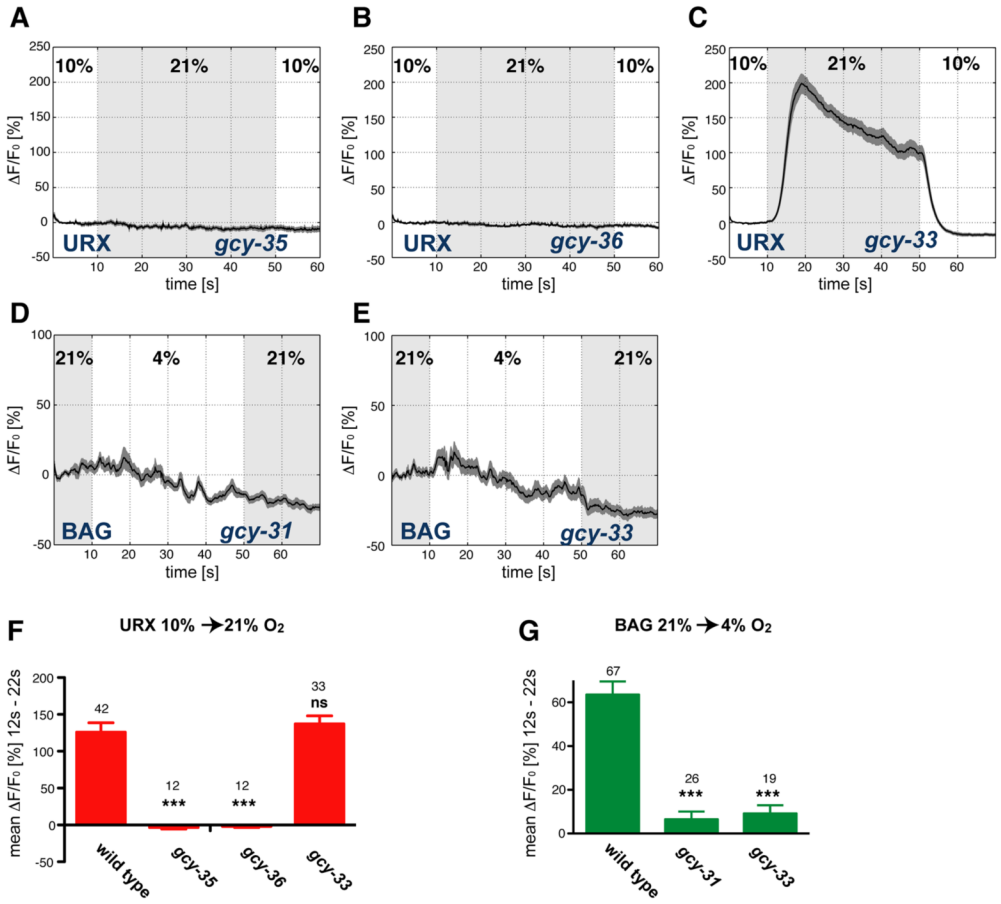

Figure 5. sGCs are required for O_2 evoked calcium transients in URX and BAG

(A–E) Measurements of neural activity by calcium imaging of URX **(A–C)** and BAG **(D,E)**. Black traces show the average percent change of G-CaMP fluorescence ($\Delta F/F_0$) and dark shading shows standard error of the mean (SEM). Concentrations were 21% and 10% O_2 **(A–C)** or 21% and 4% O_2 **(D,E). (A)** URX, *gcy-35(ok769)* mutants. **(B)** URX, *gcy- 36(db66)* mutants. **(C)** URX, *gcy-33(ok232)* mutants. **(D)** BAG, *gcy-31(ok296)* mutants. **(E)** BAG, *gcy-33(ok232)* mutants. Light grey shading indicates the intervals at 21% O_2. **(F,G)** Average $\Delta F/F_0$ from 12–22 seconds for indicated genotypes, **(F)** URX; **(G)** BAG. The data for wild type animals correspond to Figure 2D,H. Error bars show SEM. Asterisks indicate significance by one-way ANOVA with Dunnett's post-hoc test using wild type in each panel as control groups (***P<0.001, ns not significant). The numbers of recordings analyzed are indicated.

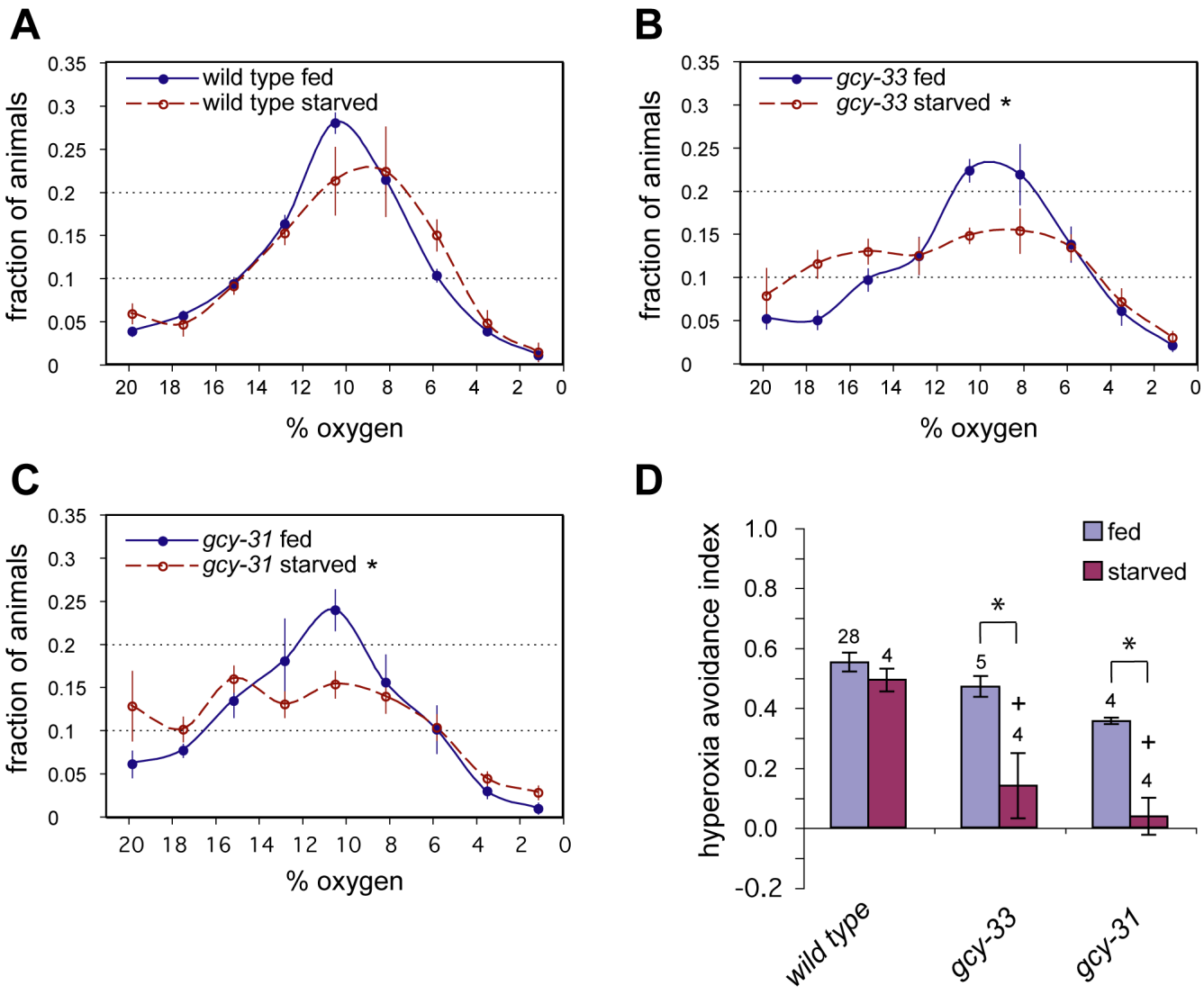

Figure 6. GCY-31 and GCY-33 promote aerotaxis in starved animals

(A–C) Distributions of fed and starved animals in gradients of 0% to 21% O_2. About 80–100 animals per assay were allowed to distribute through a device with a linear O_2 gradient, and their positions were scored after 25 minutes. Error bars indicate standard error of the mean (SEM). **(A)** Wild type. **(B)** *gcy-33(ok232)* mutants. **(C)** *gcy-31(ok296)* mutants. **(D)** The hyperoxia avoidance index describes the preferential accumulation of animals in the middle three bins (7–14% O_2) compared to the left three bins (14–21% O_2), and is calculated as [(# at 7–14%)−(# at 14–21%)]/(# in 7–21%). Error bars indicate SEM. Asterisks indicate significance by t-test, $P < 0.05$. Crosses indicate significance by one-way ANOVA with Dunnett's post test using N2 starved as control group ($P < 0.05$). The numbers of experiments performed are indicated.

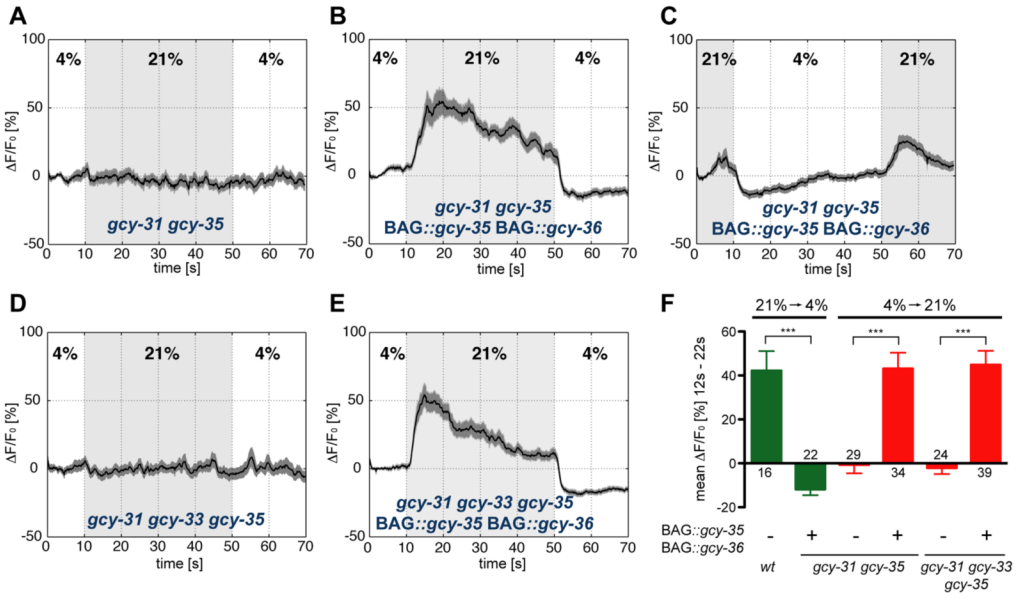

Figure 7. sGCs define neuronal oxygen specificity

(A–E) Calcium imaging of BAG neurons with altered sGC expression. Black traces show the average percent change of G- CaMP fluorescence ($\Delta F/F_0$) and dark shading shows standard error of the mean (SEM). Concentrations were 21% and 4% O_2. Light grey shading indicates the intervals at 21% O_2. **(A,B)** Calcium responses of *gcy-35(ok769); gcy-31(ok296)* **(A)** and *gcy-35(ok769); gcy-31(ok296); BAG::gcy-35 BAG::gcy-36* sGC swap animals **(B)** to O_2 upshift. **(C)** Calcium responses of *gcy-35(ok769); gcy-31(ok296); BAG::gcy-35 BAG::gcy-36* sGC swap animals to O_2 downshift. **(D,E)** Calcium responses of *gcy-35(ok769); gcy-33(ok232); gcy-31(ok296)* **(D)** and *gcy-35(ok769); gcy-33(ok232); gcy-31(ok296); BAG::gcy-35 BAG::gcy-36* sGC swap animals **(E)** to O_2 upshift. **(F)** Average $\Delta F/F_0$ (12–22 s) of animals with indicated genotypes. Error bars indicate SEM. Asterisks indicate significance by t-test (***P<0.0001). The numbers of recordings analyzed are indicated.

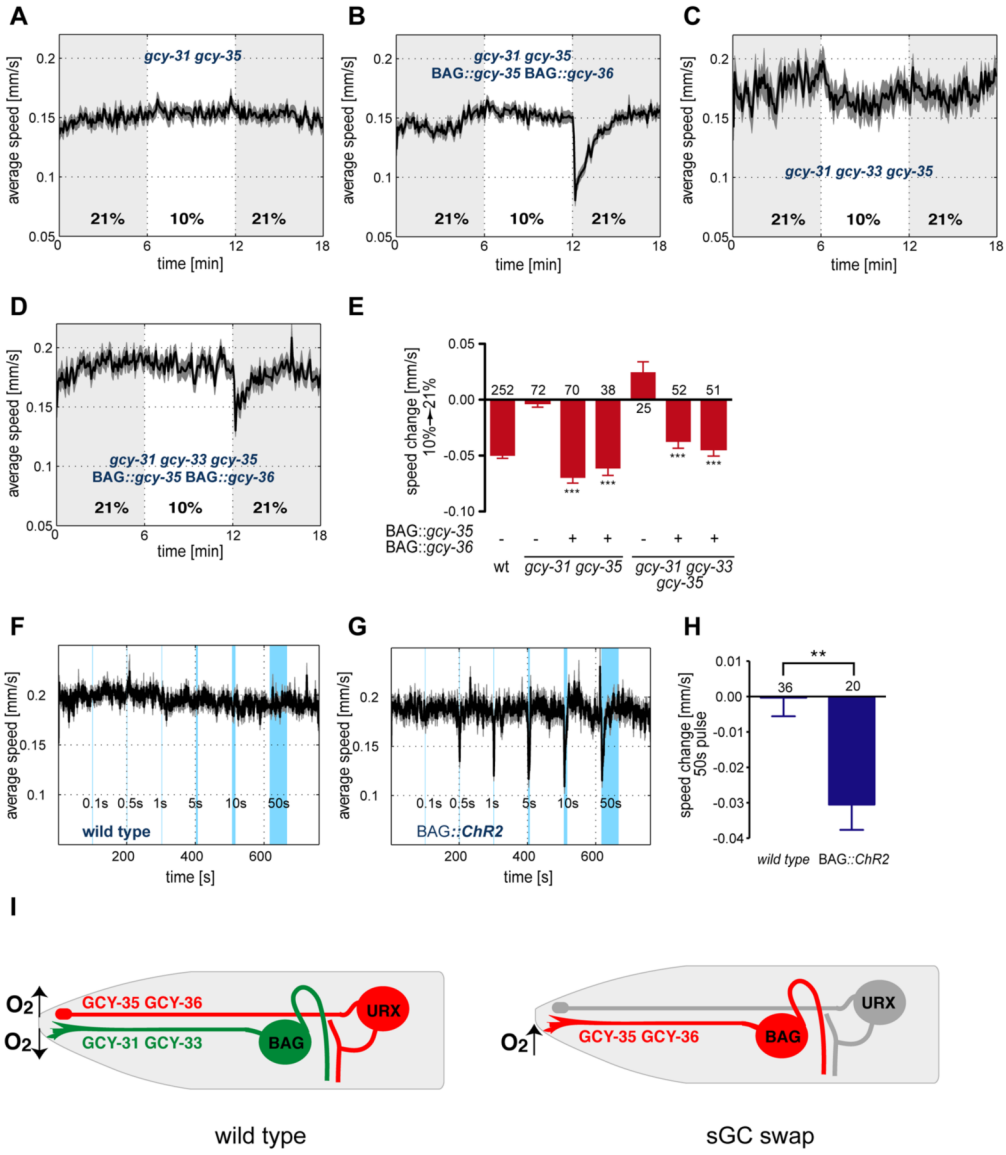

Figure 8. BAG neurons expressing β2-like sGCs mediate BAG specific behavioral responses to O_2 upshift

(A–D) Locomotion speed of animals with the indicated genotypes. Traces show average speed and shading indicates SEM. Concentrations were 21% and 10% O_2; shading marks intervals at 21% O_2. **(A)** *gcy-35(ok769); gcy-31(ok296)* double mutants. **(B)** *gcy-35(ok769); gcy-31 (ok296); BAG::gcy-35 BAG::gcy-36* sGC swap animals. **(C)** *gcy-35(ok769); gcy-33(ok232); gcy-31(ok296)* triple mutants. **(D)** *gcy-35(ok769); gcy-33(ok232); gcy-31(ok296); BAG::gcy-35 BAG::gcy-36* sGC swap animals. **(E)** Average speed changes (difference of the means of 10 second intervals before and after the switch) of animals with the indicated genotypes. Error bars indicate SEM. Asterisks indicate significance by one-way ANOVA with Dunnett's post test using the corresponding mutants in each panel as control groups (***P<0.001). The numbers of animal tracks analyzed are indicated. Wild type data are from Figure 1D. **(F–H)** Locomotion speed of control animals **(F)** or animals that express the light gated ion channel ChR2 in BAG under the BAG specific *flp-17* promoter **(G)**. Traces show average speed and shading indicates SEM. Blue shaded bars show when animals were exposed

to blue light for the indicated time intervals. **(H)** Average speed changes (difference of the means of 10 second intervals before and during the 50 second light pulse). Error bars indicate SEM. Asterisks indicate significance by t-test (P= 0.0012). The numbers of animal tracks analyzed are indicated. **(I)** Model of sensory function in URX and BAG neurons, in wild-type and sGC swap (*gcy-35(ok769); gcy-33(ok232); gcy-31(ok296); BAG::gcy-35 BAG::gcy-36)* animals. Cell bodies, sensory processes, and axons are diagrammed. Left, in wild-type animals URX is depolarized by O_2 upshift and BAG by O_2 downshift. Right, in sGC-swap animals, BAG is depolarized by O_2 upshift, and URX is silenced by the *gcy-35* mutation.